



Contents lists available at ScienceDirect

Medical Engineering & Physics

journal homepage: www.elsevier.com/locate/medengphy



The air–liquid flow in a microfluidic airway tree

Yu Song, Michael Baudoin, Paul Manneville, Charles N. Baroud*

LadHyX and Department of Mechanics, Ecole Polytechnique, CNRS UMR 7646, 91128 Palaiseau Cedex, France

ARTICLE INFO

Article history:

Received 13 January 2010
Received in revised form
28 September 2010
Accepted 4 October 2010

Keywords:

Two-phase flow
Airway tree
Liquid plugs
Microfluidics

ABSTRACT

Microfluidic techniques are employed to investigate air–liquid flows in the lung. A network of microchannels with five generations is made and used as a simplified model of a section of the pulmonary airway tree. Liquid plugs are injected into the network and pushed by a flow of air; they divide at every bifurcation until they reach the exits of the network. A resistance, associated with the presence of one plug in a given generation, is defined to establish a linear relation between the driving pressure and the total flow rate in the network. Based on this resistance, good predictions are obtained for the flow of two successive plugs in different generations. The total flow rate of a two-plug flow is found to depend not only on the driving pressure and lengths of the plugs, but also the initial distance between them. Furthermore, long range interactions between daughters of a dividing plug are observed and discussed, particularly when the plugs are flowing through the bifurcations. These interactions lead to different flow patterns for different forcing conditions: the flow develops symmetrically when subjected to constant pressure or high flow rate forcing, while a low flow rate driving yields an asymmetric flow.

© 2010 IPEM. Published by Elsevier Ltd. All rights reserved.

1. Introduction

The lung is a dynamic organ where mechanical stresses play an important biological role. These stresses may arise in particular from the presence and transport of liquids within the airway tree. While liquid is always present on the inner surfaces of the pulmonary paths, it can form discrete plugs that occlude the airway in pathological situations [1]. Indeed, many respiratory pathologies, such as asthma, pneumonia, or respiratory distress syndrome, may involve the blockage of the airways by liquid plugs which impede the flow of air. Moreover, flows associated with the movement or rupture of liquid plugs can cause damage to endothelial cells which line the lung surface [2,3].

In addition to these pathologies where occlusion by the pulmonary fluids can occur, the instillation of liquid plugs into the pulmonary airway is common in medical treatments such as partial liquid ventilation and drug delivery [4]. It is of vital importance, for instance, in the case of Surfactant Replacement Therapy, where surfactant is injected as a liquid bolus into the lungs of premature neonates [5]. In these cases of drug delivery, the only available control over the plug distribution is at the entrance of the network, at the level of the patient's trachea. Once the bolus is injected, little is known about the ultimate distribution of liquid within the pulmonary tree, although some studies have attempted to predict surfactant dispersion by numerical or experimental models [6,7].

Variations in the paths taken by daughters of the initial surfactant plug may account for the inconsistent responses observed in such therapies [5].

One of the difficulties that arise is due to the interactions between the immiscible interfaces and the complex geometry of the lung. Indeed, the presence of surface tension introduces a nonlinear relationship between pressure drop and flow rate in a particular branch, through the addition of Laplace pressure terms [8,9]. While these nonlinearities already appear in flow through straight channels [10], they are amplified when plugs pass a bifurcation since the interfaces must strongly deform in this case [9]. This can lead to the existence of local blockage if the pressure is below a threshold value, or to plug rupture if the plug length is too small.

Microfluidics has already been proposed as a way to model branching geometry of the lung, at least in the generations where gravity and inertial effects are negligible [11]. These regions of the lung are characterized by length scales below the capillary length and small Reynolds numbers. The capillary length L_C , i.e. the scale below which the effects of gravity become small compared with surface tension effects, is generally around 2 mm for most liquids. The Reynolds number compares the effects of fluid inertia with viscous effects through the relation $Re = \rho_l U D / \eta$, where ρ_l is the liquid density, U is a characteristic velocity, D is the airway diameter, and η is the fluid viscosity. The two criteria $D < L_C$ and $Re < 1$ are met in the lung for a large range of generations, starting from about generation 9 to the respiratory bronchioles, around generation 20 [12]. The ability to fabricate complex microfluidic geometries using photo-lithography techniques therefore opens a wide range of pos-

* Corresponding author. Tel.: +33 169335261; fax: +33 169335292.
E-mail address: baroud@ladhyx.polytechnique.fr (C.N. Baroud).

sibilities for addressing questions of liquid distribution that are relevant for pulmonary flows, in the presence of different additional physical phenomena.

Below, we study the motion of liquid plugs in a connected tree of microchannels. We begin with a description of the experimental setup in Section 2. In Section 3, we derive an empirical relation for the resistance to flow due to a single plug in the network and show that this relation generalizes well for the case of a train of two plugs. Further, different behavior is observed for pressure vs. flow rate driving as the plug flows further into the network, since the resistance to flow is modified by the passage through successive bifurcations.

2. Experimental setup

Our experiments are conducted in a network consisting of branching microchannels that have rectangular cross-sections, as shown in Fig. 1. Soft lithography techniques are employed to make the channels of polydimethylsiloxane (PDMS) [13]. A thin flat layer of PDMS is spin-coated on a glass microscope slide and the channels are bonded on this PDMS layer in order to guarantee identical boundary condition at all four channel walls.

The network inlet consists of a Y-junction connected to the first generation for creating and injecting liquid plugs into the network. One inlet of the Y-junction is connected to a syringe filled with perfluorodecalin (PFD) and the syringe can be pushed by a pump. PFD is a fluorocarbon whose viscosity and surface tension are $\eta = 5 \times 10^{-3}$ Pa s and $\gamma = 20 \times 10^{-3}$ N/m, respectively. It presents good wetting properties on PDMS and does not swell the channels. Through the second inlet of the Y-junction, the air goes into the network and a constant driving is applied between the first and the last generations. Either constant pressure or constant flow rate can be applied. When pushing at constant pressure, the inlet of the air is connected to a computer-controlled pressure source (FLUIGENT, MFCS-8C). To apply a constant flow rate, a syringe is filled with water and connected to the air inlet through a flexible tube. Only a small volume of air near the network entrance is left in the tube in order to reduce the effects

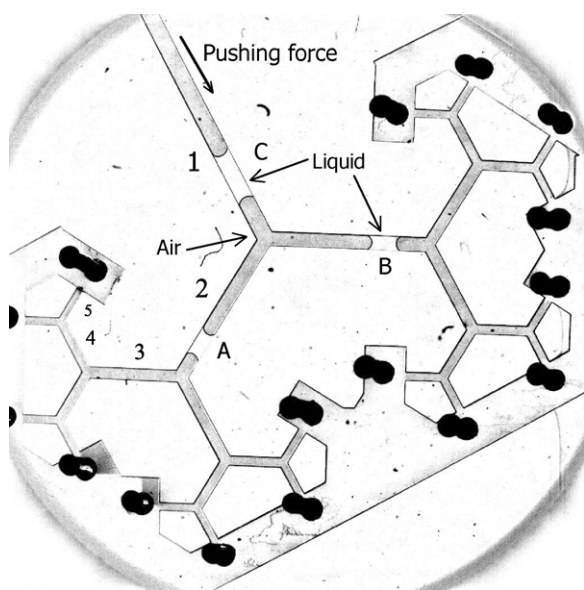


Fig. 1. Microscope image of the microfluidic network with five generations. Generations are numbered with Arabic numerals. The two early plugs (A and B) in generation 2 are the daughters of the first plug. A second plug (C) is moving in the first generation.

Table 1
 Experimental conditions.

Number of plug(s)	Driving Condition
1	Pressure: $P_{dr} = 150, 250, 400$ Pa
1	Flow rate: $Q_{dr} = 2, 5, 20$ $\mu\text{L}/\text{min}$
2	Pressure: $P_{dr} = 500$ Pa

of air compressibility. A syringe pump ensures a constant flow rate of the water which then pushes the air into the network. Driving conditions for the experiments in this paper are given in Table 1.

The height of all the branches in the network is 50 ± 2 μm and the width of the branch in the first generation is 720 μm . Channel widths of successive generations w_i decrease at a constant rate $w_{i+1} = \rho w_i$, where $\rho = 0.83$ is a constant parameter and the subscript denotes the generation number. This value of ρ preserves the ratio of mean diameters observed in the pulmonary airway [12]. It gives a width 342 μm for the last generation. The channel lengths also decrease linearly with the generation number, with a ratio 0.6 . This value was chosen to preserve the ratio of plug length to branch length at each generation, thus reducing the number of variables in the problem, if the plugs divide symmetrically at the bifurcations. PFD plugs (bright regions) surrounded by air (gray regions) are indicated in Fig. 1. The plugs are injected into the first generation and pushed through the network, dividing into two daughters at every bifurcation. At the exits of the last generation, sixteen holes (black in Fig. 1) are punched to fix the exit condition at atmospheric pressure.

Experiments are recorded with a high speed camera (Photron Fastcam, 1024 PCI) through a stereomicroscope at $0.7\times$ magnification. The resolution of the camera is 1024×1024 pixels, which yields 1 pixel for 24.8 μm . For the single plug experiments, images are taken at different rates (varying from 30 to 125 images per second) according to the driving conditions, thus ensuring that the plug positions can be traced with a good resolution. For two successive plugs under constant pressure driving, 125 images per second are recorded. From the image sequences thus obtained, the positions x_r of the rear interface of the plug are manually recorded while the plug is traveling in the network. Based on these measurements, the plug velocity is calculated as $U = [x_r(t) - x_r(t - dt)]/dt$, where dt is the time step between successive images. The fluid deposition on the walls is neglected in the calculation since it does not affect the flow significantly in our experimental conditions.

3. Movement in the straight sections

In this section, we focus on the velocity of a plug pushed at a constant pressure as it travels in the straight channels between two successive bifurcations. We first study the case of a single plug and its daughters in the network, then build a relation reproducing the results and show that it can be applied to the case of two successive plugs and their daughters.

3.1. A single plug in the network

A single plug is injected into the network and then pushed at a constant pressure P_{dr} . It divides into two at every bifurcation and velocities of all its daughters, measured in each branch, are recorded according to their position in the network (generation numbers i). The daughter plugs are constantly subjected to the same pressure difference and should therefore all move at the same speed which, in addition, should be constant during their passage in their respective branches. Variations from branch to branch and within a branch, to be attributed to imperfections in the micro-

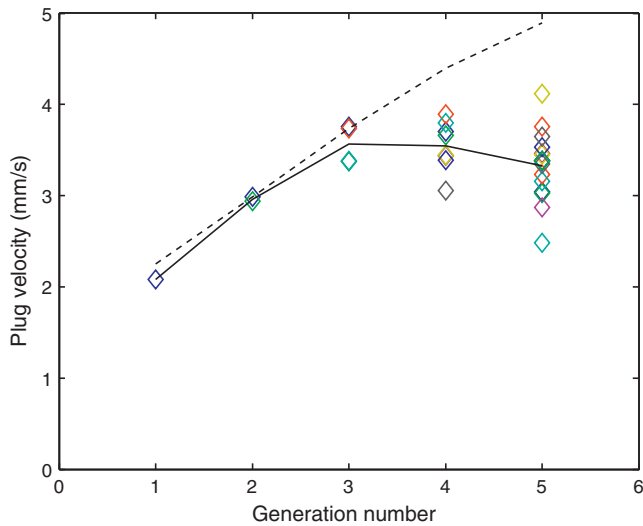


Fig. 2. Average plug velocity as a function of the generation number i (driving pressure 250 Pa). Symbols correspond to values recorded in each branch and the solid line to their average. The prediction from a previous study [9] is shown as a dashed line.

fabrication, are observed however. As the channels get narrower, the flow becomes more sensitive to wall conditions, which brings bigger separations between data points in later generations. For each generation number i , values corresponding to the 2^{i-1} individual time-averages of the plug velocities are plotted in Fig. 2. The solid line drawn through these points thus gives the average value obtained over the 2^{i-1} branches.

At this stage, it is interesting to compare these observations to the theoretical prediction that could be made from the study of plug motion in straight channels in microfluidics conditions [9]. The formula in Eq. (11) of Ref. [9] is used to compute the velocity in all the generations by assuming that plugs divide equally at each bifurcation while taking into account the narrowing of the channels $w_i = w_1 \rho^{i-1}$, hence $L_i = L_1 / (2\rho)^{i-1}$. The result is given as a dashed line in Fig. 2, from which it is immediately seen that the plugs experience a resistance larger than predicted as they progress in the network. Since the formula is well validated in the case of long plugs, we attribute the discrepancy to the exponential shortening of the plugs with the generation number: for the experiment corresponding to the data in Fig. 2, the plug length in the last generation is $L_5 = 300 \mu\text{m}$ while the channel width is $w_5 = 342 \mu\text{m}$. Plugs are therefore comparatively short and the resistance is underestimated in the last generations.

The limitations of the theory led us to develop an empirical relation that we now describe. As for an electrical network, we define a resistance $R_i L_i$ associated with the presence of a daughter plug of length L_i in generation i , where the role of the voltage is played by the driving pressure P_{dr} and the role of the current intensity by the volumetric flow rate in each branch of that generation Q_i . We can therefore write $P_{dr} = R_i L_i Q_i = R_i L_i Q_i N_i$, where $N_i = 2^{i-1}$ is the number of branches in that generation and $Q_t = Q_i N_i$ is the total flow rate in the network. We assume further that each plug divides into two daughters of essentially equal lengths at every bifurcation, which is consistent with experimental observations, $L_i = L_1 / (2\rho)^{i-1}$. Flow rate Q_i is calculated as $Q_i = U_i h w_i$, U_i being the plug velocity in that generation. The values of R_i can be computed from the measurements since the driving pressure, the initial length of the plug and the flow rate based on velocity measurements are known. They are found to decrease with the generation number, as shown in Fig. 3. This leads to an increase in the total flow rate Q_t as the plug reaches later generations (symbol \blacklozenge in Fig. 4).

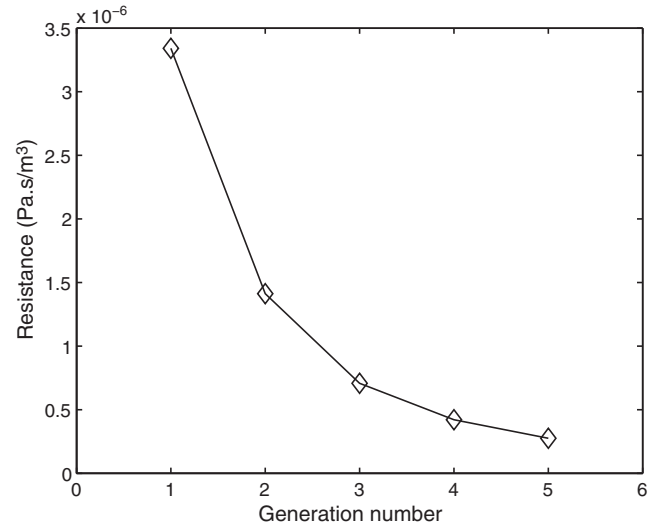


Fig. 3. Dependence of the resistance on the generation number.

3.2. Two successive plugs

The relation just defined now allows us to analyze the dynamics when two plugs are injected successively. Like for two resistors mounted in series, the relation between the driving pressure and the volumetric flow rate can be written as $P_{dr} = R_i^{[1]} L_i^{[1]} Q_t^{[1]} + R_j^{[2]} L_j^{[2]} Q_t^{[2]} = (R_i^{[1]} L_i^{[1]} + R_j^{[2]} L_j^{[2]}) Q_t$, where the superscripts ‘[1]’ and ‘[2]’ denote the first and the second plugs and the subscripts ‘ i ’ and ‘ j ’ indicate the position of the plugs in the network by the corresponding generation numbers. Using the values of R_i determined above and the initial lengths of two plugs, $R_i L_i$ can be computed. Flow rates for a two-plug train for the driving pressure $P_{dr} = 500 \text{ Pa}$ are compared to the experimental findings in Fig. 4. Satisfactory agreement is obtained, indicating that the linear description of the flow in the network gives a good approximation in the current conditions.

Notice that although the lengths of the plugs and the driving pressure are kept the same, the total flow rate displays a clear dependence on the distance between the two plugs, as shown in Fig. 4. When the plugs get further apart, a higher flow rate is

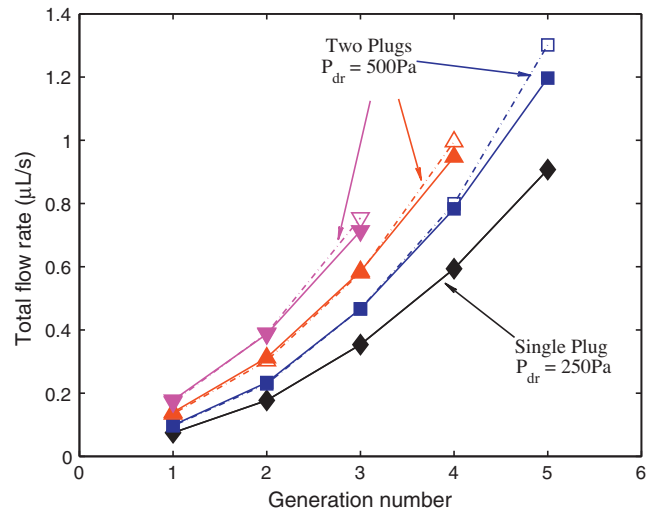


Fig. 4. Evolution of the total flow rate in a single plug experiment (\blacklozenge) (driving pressure $P_{dr} = 250 \text{ Pa}$) and two-plug experiments ($P_{dr} = 500 \text{ Pa}$) when they always flow in the same generation (\square), in two successive generations (\triangle) and with a separation of one generation (∇). Open symbols denote experimental data and closed ones are values derived from the linear law.

observed. This can be understood by noting that the resistance due to the downstream plug decreases with generation number and thus the sum $(R_i^{[1]}L_i^{[1]} + R_j^{[2]}L_j^{[2]})$ also decreases.

4. Passage through a bifurcation and long range interactions

The passage of a plug in a bifurcation leads to highly nonlinear effects because of the strong modification of the shape of the interface. We begin by considering the details of the passage of a plug through a bifurcation before turning to how the behavior of one plug influences the passage of plugs elsewhere in the network.

4.1. One plug in one bifurcation

Consider a plug that just arrives at a bifurcation, as sketched in Fig. 5(a). The curvature of the front interface decreases before the rear one is affected by the bifurcation, which introduces a capillary pressure difference across the plug. This is a three-dimensional problem and the biggest curvature of the interface exists in the direction perpendicular to the plane of the network. However, we assume that the capillary pressure difference is mainly driven by curvature differences in the plane of the network. The pressure difference P_{cap} between the rear and front interfaces can be expressed as $P_{cap} = P_r - P_a = \gamma/r_r - \gamma/r_a$, where P_r, P_a denote the capillary pressures at the receding and advancing interfaces and r_r, r_a are the signed radii of curvature of the interfaces in the plane of the network. Before the plug touches the opposite wall, we have $r_a > r_r$ and r_a increases as the plug advances. So P_{cap} acquires increasing positive values. There exists a threshold pressure necessary to push a plug through a bifurcation, which is estimated as the maximum value of P_{cap} : $P_{thr} = P_{cap,max} = \gamma/r_r - \gamma/r_{a,max}$ where $r_{a,max}$ is the maximum possible value of r_a , reached just before the front interface touches the corner of the opposite wall. Beyond this point, P_{cap} becomes negative ($r_a < r_r$) and pulls the daughter plug (Fig. 5(b)). When the plug has fully passed the bifurcation, P_{cap} cancels ($r_a \approx r_r$).

The threshold pressure P_{thr} can be computed from the network geometry:

$$P_{thr} = \frac{2\gamma \cos \theta}{w_i} - \frac{\gamma(\cos \theta - \sin \alpha)}{w_{i+1}} \quad (1)$$

where θ is the contact angle of PFD on PDMS (around 23°) and the bifurcation half-angle, α , is half the angle between the two branches of the same generation. Here $\alpha = 60^\circ$ yields the threshold pressure $P_{thr} = 51, 61, 74$ and 89 Pa for the first to the fourth bifurcations, respectively. Although the values of P_{thr} depend on the value of the contact angle θ , a difference of 23° in the contact angle only changes the threshold by 2 Pa.

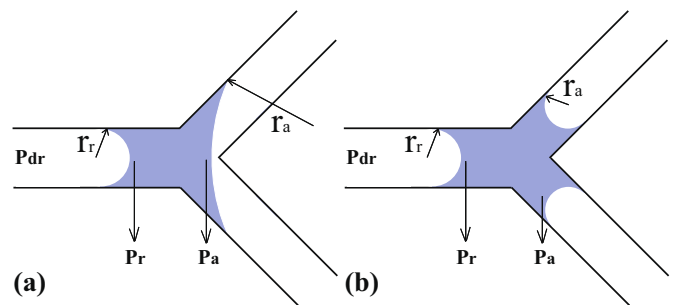


Fig. 5. Passage through a bifurcation. (a) A plug arrives at the bifurcation. The radius of curvature r_a is bigger than r_r and increasing while the plug is advancing. (b) After the front interface touches the next generation, r_a becomes smaller than r_r (notice that here $2\alpha = 90^\circ$ for convenience).

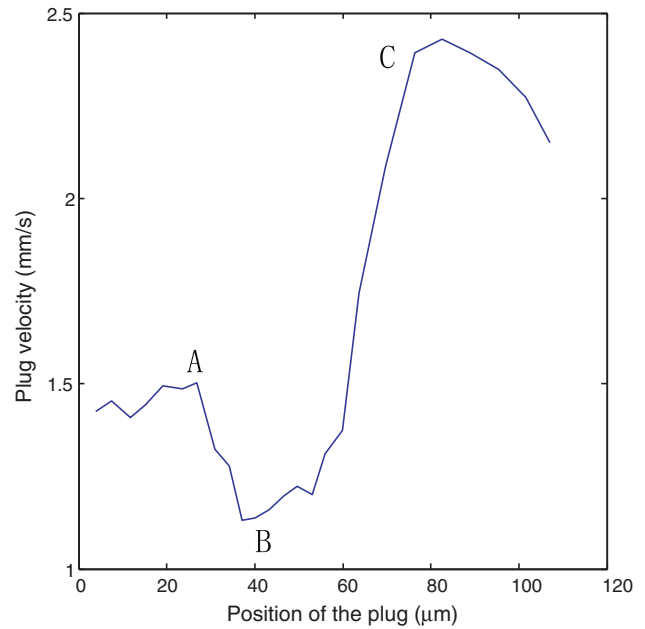


Fig. 6. Experimental measurements of plug velocity during the passage through a bifurcation. The position of the plug is defined as that of its rear interface.

When the plug is pushed at a constant pressure, the pressure difference across the plug can be expressed as $\Delta P = P_{dr} - P_{cap}$. The variation in P_{cap} will lead to variations of ΔP and also of the velocity of the plugs as they advance. In order to push a plug through a bifurcation, ΔP has to remain positive during the passage. This implies that the driving pressure has to be larger than the threshold pressure. Meanwhile, the velocity variations during the passage should account for the appearance of P_{cap} , which modifies the value of the effective driving pressure as ΔP .

Measurements of the velocity of a particular plug are shown in Fig. 6 when it is pushed at $P_{dr} = 250$ Pa and passes the second bifurcation in the network. The plug initially slows down after it enters the bifurcation (position A), after which its velocity rises quickly as the front interface reaches the opposite wall (position C), since $P_{cap} < 0$ and ΔP increases. Accordingly the passage of a plug through a bifurcation is always associated with a large spike in the velocity.

When the plug is forced at a constant flow rate, if the passage can be treated as a quasi-static process, we may write that $\Delta P = P_{cap}$ [14]. Variations in P_{cap} will therefore induce variations in the pressure upstream of the plug position such that ΔP will increase until the plug touches the opposite wall, where it rapidly switches to a negative value which pulls the plug into the daughter channels. The largest value reached by ΔP is $\Delta P = P_{thr}$.

4.2. Plug interactions

The connectivity of the branching tree implies that local pressure variations will lead to long range effects across different regions of the network. The fundamental unit to understand these interactions is shown in Fig. 7, where two daughters (I and II) of the same plug arrive at two bifurcations nearly simultaneously.

Assume that plug I touches the opposite wall slightly earlier than plug II. Then, its velocity as well as the flow rate in that branch increase according to the above analysis. In case of constant pressure forcing, the driving condition for plug II is not modified; this plug also slows down and then speeds up as it crosses the bifurcation, independently of plug I. This is no longer the case if the plugs are pushed at constant flow rate Q . When plug I passes the bifurcation

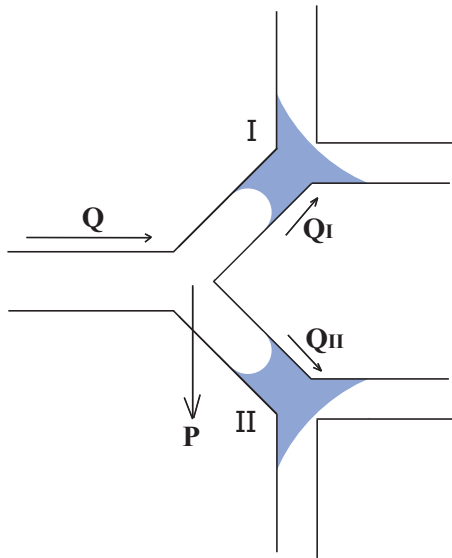


Fig. 7. The fundamental unit of long range interactions between two plugs.

shown in Fig. 7, the flow rate Q_I increases, forcing Q_{II} to decrease in order to conserve the value of $Q = Q_I + Q_{II}$. In fact, Q_{II} may become zero or even negative, which means that plug II may stop or even move backwards, depending on the value of Q .

5. Results

The flow behavior is studied by tracking the positions and velocities of daughter plugs along the paths shown in Fig. 8. In these experiments, a single plug is injected into the network and forced to divide into two at every bifurcation.

5.1. Constant pressure driving

A time sequence showing the successive divisions is shown in Fig. 9, when the plug is pushed at a constant driving pressure $P_{dr} = 250$ Pa. Only half of the network is shown for clarity. As seen in these images, the plug positions may vary slightly across the dif-

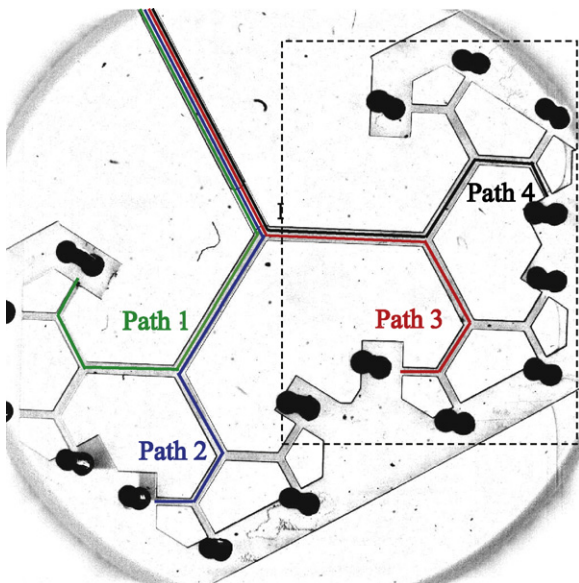


Fig. 8. Paths along which the plug positions and velocities are measured. The dashed box indicates the zone that is displayed in Figs. 9 and 11.

ferent generations but they mostly advance in synchrony through the bifurcations and across generations. These results are typical of many different experiments. A more quantitative measure of this synchronous flux is given by measuring the plug velocities as functions of time along the four paths, as shown in Fig. 10. As the daughter plugs advance in the network, their number increases and their velocities vary according to the analysis in Section 3.

The spikes that appear in the velocity time series are the signatures of passages through the bifurcations, as explained above. By tracking the moment at which the spikes occur along each of the different paths, we see that the plugs reach the bifurcations and divide at roughly the same time. This is in spite of imperfections in the network which lead to slight asymmetry in the divisions and thus yield plugs of variable sizes. Moreover, a careful examination of the time series reveals small differences in the passage times through the second bifurcation. However, this difference is not amplified in later generations and the plugs all continue in a steady fashion. The flow remains globally symmetric during its evolution.

5.2. Constant flow rate driving

When the experiments are repeated by pushing the plug at a constant flow rate, the behavior may be strongly modified. In the experiment shown in Fig. 11, the driving flow rate is $Q_{dr} = 2 \mu\text{L}/\text{min}$ and two daughters are observed as they advance simultaneously in generation 2 (image (b)) but this synchrony is broken when they reach the bifurcation. At this stage, only one of the daughters divides and its daughters continue to flow in generation 3 (image (c)). However, the upstream plug catches up with its sister which gets blocked at the next bifurcation due to the higher threshold pressure.

The velocities of the plugs are displayed in Fig. 12 along the same paths as above. Due to flow rate conservation in the network, the plugs adjust their velocities while advancing and the acceleration in one path leads to a deceleration in the others. Here, an uneven division, which introduces daughters of different lengths, leads to significant velocity variations since a shorter daughter is easier to push forward than a longer one. Velocity differences are visible, for instance, in the case of the two daughters of the initial plug as they flow in generation 2: while the one in paths (3, 4) speeds up, the one in paths (1, 2) must slow down.

After one daughter passes a bifurcation and divides, a flow rate increase in the corresponding branches results in a slowing down of other daughters which become stuck at the bifurcations. Once the early plug that has divided reaches the next bifurcation, the threshold pressures at two successive bifurcations have to be compared and the plug with the lowest threshold will advance first. In this network, the threshold increases with generation number, which implies that the late plugs can catch up with the early ones. The most downstream plug must therefore wait at the bifurcation for all other plugs to reach the same bifurcation level before it can continue its journey. This is shown in the velocity evolution in Fig. 12, by the segments with zero velocities before the passage of a bifurcation.

At constant flow rate forcing $Q_{dr} = 2 \mu\text{L}/\text{min}$, the air–liquid flow therefore remains symmetric but evolves through discrete steps. Plugs are never more than one generation apart due to the increasing threshold pressure, but they spend long periods of time stationary at bifurcations, waiting for plugs in the other branches to catch up.

5.3. Flow patterns in the network

Results of experiments repeated at different driving conditions are summarized in this section. As shown earlier, the flow is synchronous at $P_{dr} = 250$ Pa, but turns out to be asynchronous at

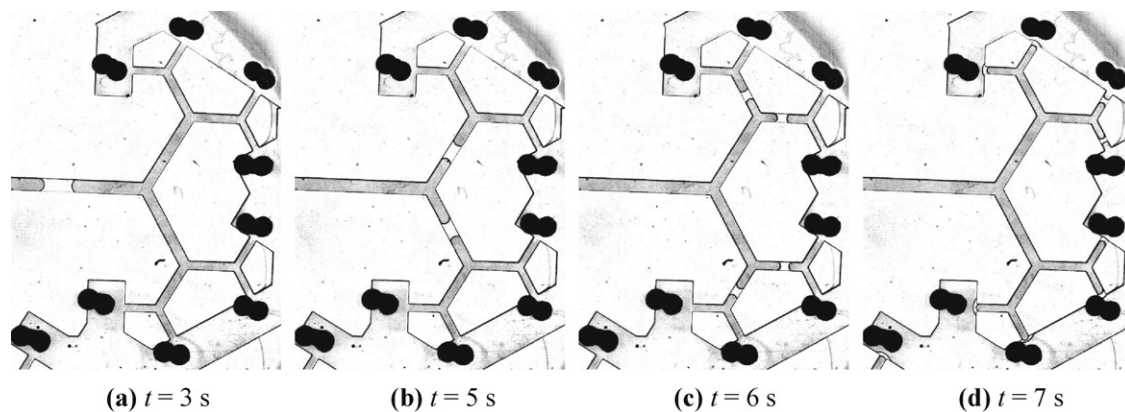


Fig. 9. Image sequence for the half network, obtained from the experiment of constant pressure driving.

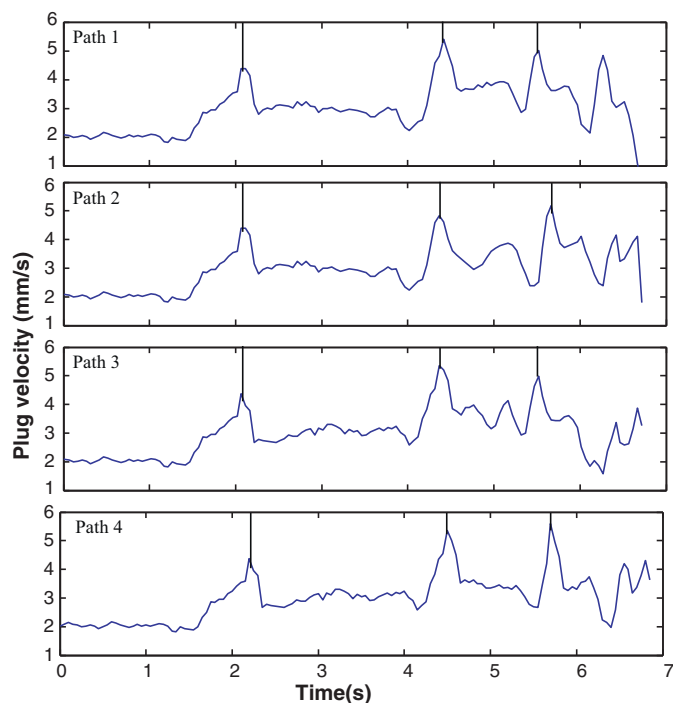


Fig. 10. Velocity variations along four paths under a constant pressure driving $P_{dr} = 250$ Pa. The vertical line indicates the time when the plug passes a bifurcation.

$Q_{dr} = 2 \mu\text{L}/\text{min}$. However, the flow pattern depends on not only the type of the driving condition but also the value of driving force.

The behavior described above can be summarized by measuring the time Δt_i separating the first and last plug divisions at a particular depth in the network. We normalize this time difference by the mean time taken to travel through the following generation (T_{i+1}) and write the normalized time $\overline{\Delta t}_i$. A value of $\overline{\Delta t}_i < 1$ indicates that the plugs advance nearly simultaneously through the generation $i + 1$, while a value of $\overline{\Delta t}_i > 1$ implies that some plugs only divide once the early ones have already reached the next bifurcation. The results for different experiments are shown in Fig. 13, where each data point corresponds to an average over several experimental realizations.

Two distinct behaviors are observed. The division times for constant flow rate driving are above 1 at the second and third bifurcations for $Q = 2 \mu\text{L}/\text{min}$ and at the third bifurcation for $Q = 5 \mu\text{L}/\text{min}$. This confirms that plugs pass one by one, waiting for each other to reach the next bifurcation. The transition to $\overline{\Delta t}_i > 1$ occurs when the pressure necessary to ensure the constant flow rate decreases below the local threshold, as described in Ref. [14]. Note that the values of $\overline{\Delta t}_i$ increase with generation number here because the number of sister plugs increases and since they must pass separately. In contrast, constant pressure driving yields values of $\overline{\Delta t}_i$ that are significantly below 1, indicating that plug divisions are nearly synchronous. This is the case for all of the data recorded here except for the lowest pressure value, at which $\overline{\Delta t}_i \sim 1.3$. This can be attributed to imperfections in the microfabrication. Indeed, depth variations of the channel, due to the uncertainty in the photolithography process, can lead to pressure differences between the front and the rear of a plug. When combined with low values of the

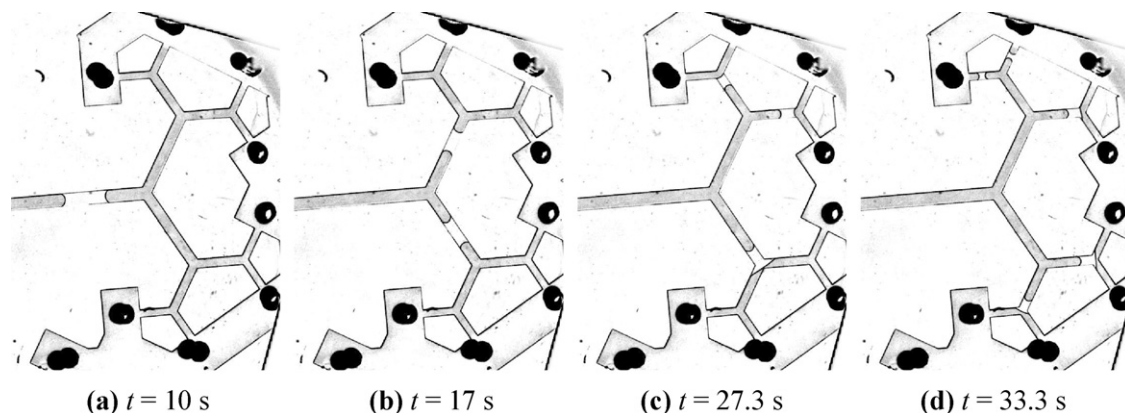


Fig. 11. Image sequence for the half network, obtained from the experiment of constant flow rate driving.

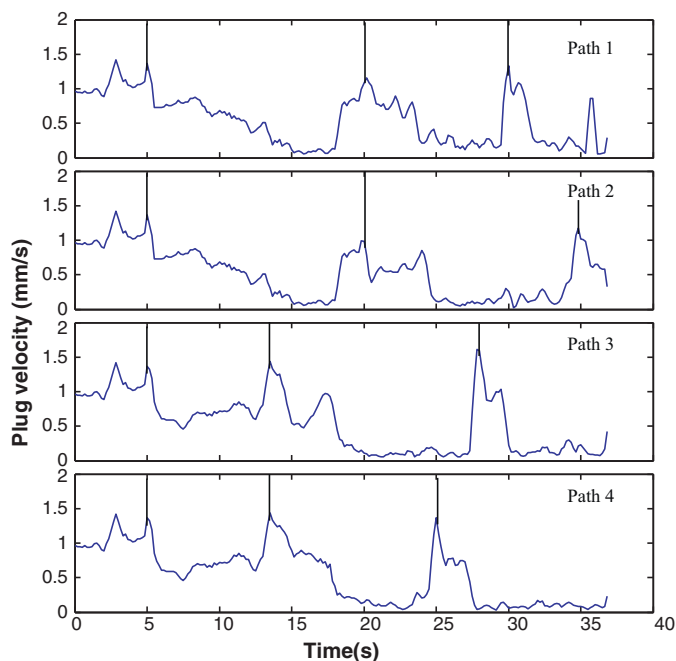


Fig. 12. Velocity evolutions along four paths under the constant flow rate $Q_{dr} = 2 \mu\text{L}/\text{min}$. The vertical line indicates the time when the plug passes a bifurcation.

driving pressure compared with the threshold to pass a bifurcation, these can result in small values of ΔP , which imply that some plugs advance very slowly through particular bifurcations.

For large driving flow rate (e.g. $Q = 20 \mu\text{L}/\text{min}$) and pressures ($P_{dr} > 150 \text{ Pa}$), the plug movement is synchronous in both methods, as seen by the small values of Δt_i . This can also be observed by plotting the positions of the plugs as a function of time, as shown in Fig. 14. In this figure, the position of the rear interface along four representative paths is plotted and all four divide simultaneously both for constant flow rate and constant pressure. However, the distance curves display different evolutions, which allows us to distinguish the driving conditions. While the plugs slightly accelerate as a function of generation number in the case of pressure forcing,

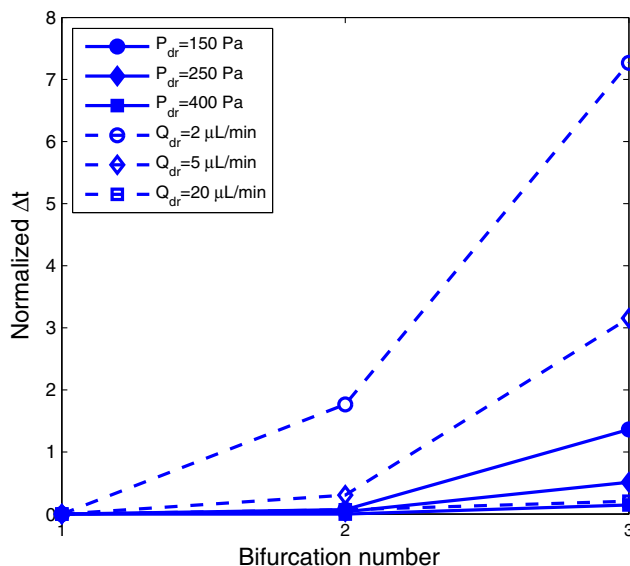


Fig. 13. Time difference of daughters' passage through bifurcations of the same level, data normalized to the average traveling time in the next generation.

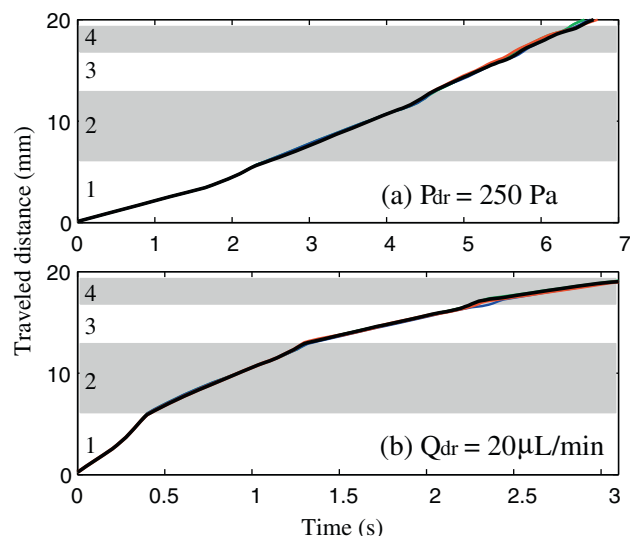


Fig. 14. Distance traveled by daughter plugs along four paths in the network. The shaded and non-shaded areas represent successive generations as labeled on the right of the y-axis and the line color is used to indicate the corresponding path shown in Fig. 8. (a) Driving condition $P_{dr} = 250 \text{ Pa}$. (b) Driving condition $Q_{dr} = 20 \mu\text{L}/\text{min}$.

they clearly decelerate in the case of flow rate driving, since the number of daughters increases and the flow is distributed over a larger area.

This information can be summarized by measuring the time (T_i) spent traveling in the straight sections in each generation. This is shown in Fig. 15, where each data point is the average over all the plugs in a given generation, averaged over several experimental realizations. T_i is normalized by the total time for an experiment, i.e. the time from the initial plug entering the first bifurcation to the last daughter passing the last bifurcation. For pressure driving, we observe that the time spent in the straight channel decreases as the plugs advance. Since the plug velocity decreases more slowly than the channel length, it takes a shorter time to pass the branch in the later generations. In the case when the plug is pushed at a high flow rate, the travel time remains constant with generation number because the decrease in plug velocity evolves in the same way as the channel length. This result is true by construction and holds for any value of ρ .

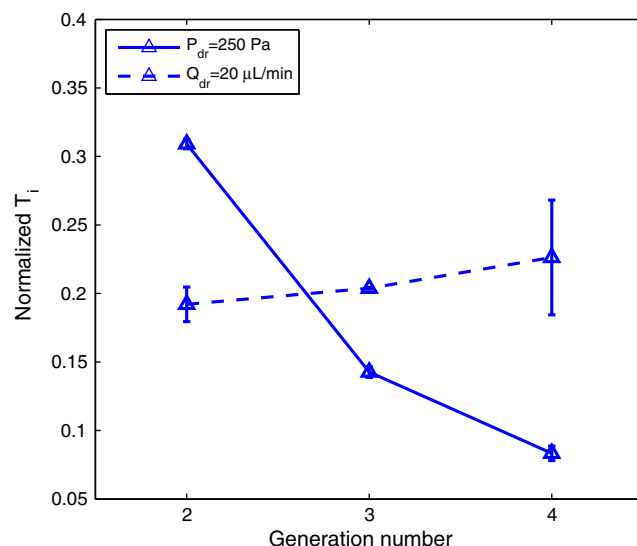


Fig. 15. Comparison of traveling time in each generation for pressure and high flow rate forcing. Both yield symmetric flow patterns.

6. Summary and discussion

In investigating the flow of liquid plugs in a branching network, an empirical relation expressing the pressure–flow rate evolution is derived from the motion of a single plug and found to account for the resistance of the network to the flow of liquid. Given the initial condition of the experiments, e.g. driving pressure and plug lengths, this relation quantitatively predicts the flow rates in the presence of a train of two plugs. This empirical relation indeed provides a better prediction of the flow of a train of plugs than the physical model presented in Ref. [9].

When two successive plugs are separated by a large distance in the network, the resistance associated with the downstream plug is small compared to the resistance of the upstream liquid. This implies that the flow rate in the network is essentially fixed by the upstream plug and the downstream plug perceives a constant flow rate forcing, even if the actual driving condition is through pressure. This may modify the flow distribution in the branching tree through inter-generation effects, which are expected to feed back on the flow everywhere in the network.

Furthermore, the passage through a bifurcation induces strong variations in the capillary pressure jumps across the air–liquid interfaces, which has a major impact on the flow through the branching channels. When considering a single bifurcation, this leads to large variations in the velocity at which the plug advances. It also leads to the existence of a threshold value of the driving pressure necessary to push the plug. A similar threshold is expected to exist in the case of the circular tubes forming the pulmonary airway tree, although its value will strongly depend on the details of the geometry at the bifurcation. Nevertheless, the presence of threshold pressures will have a similar effect on the global organization of flow in the lung as observed in our experiments. Finally, although the threshold values may be small compared with the driving pressure, a sufficiently deep airway tree will always lead to regions in which the local pressure becomes comparable with the value of the threshold.

The influence of the driving condition on the plug propagation in the network has also been explored. The nonlinear pressure–flow rate relation at a bifurcation induces strong long range interactions between plugs in different parts of the network. This is particularly visible in the case of driving the fluids with a low flow rate, in which case some plugs can stop at bifurcations and wait for long periods of time while others continue to advance. Nevertheless, symmetric filling of the network is observed in both conditions. Finally, syn-

chronized filling can be achieved at high pressure and high flow rate driving although different flow evolutions are observed at two conditions. A better understanding of the filling of a branching tree and of the long range interactions in it should lead to improved models of liquid dispersion in the lung, which is an important problem in view of its application to pathology and drug delivery.

Acknowledgments

The authors thank FLUIGENT Company for their kind support. Michael Baudoin was funded by the ANR under the “Santé-Environnement et Santé-Travail” programme.

Conflict of interest

All the authors declare that there is no conflict of interest associated with this work.

References

- [1] Grotberg J. Pulmonary flow and transport phenomena. *Annu Rev Fluid Mech* 1994;26:529–71.
- [2] Bilek A, Dee K, Gaver D. Mechanisms of surface-tension-induced epithelial cell damage in a model of pulmonary airway reopening. *J Appl Physiol* 2003;94(2):770–83.
- [3] Huh D, Fujioka H, Tung Y-C, Futai N, Paine R, Grotberg JB, et al. Acoustically detectable cellular-level lung injury induced by fluid mechanical stresses in microfluidic airway systems. *Proc Natl Acad Sci USA* 2007;104(48):18886–91.
- [4] Leach C, Greenspan J, Rubenstein S, Shaffer T, Wolfson M, Jackson J, et al. Partial liquid ventilation with perflubron in premature infants with severe respiratory distress syndrome. *N Engl J Med* 1996;335(11):761.
- [5] Engle WA, the Committee on Fetus & Newborn. Surfactant-replacement therapy for respiratory distress in the preterm and term neonate. *Pediatrics* 2008;121(2):419–32.
- [6] Espinosa F, Kamm R. Bolus dispersal through the lungs in surfactant replacement therapy. *J Appl Physiol* 1999;86(1):391–410.
- [7] Cassidy KJ, Gavriely N, Grotberg JB. Liquid plug flow in straight and bifurcating tubes. *J Biomech Eng* 2001;123(6):580–9.
- [8] Bico J, Quéré D. Falling slugs. *J Colloid Interface Sci* 2001;243(1):262–4.
- [9] Ody CP, Baroud CN, de Langre E. Transport of wetting liquid plugs in bifurcating microfluidic channels. *J Colloid Interface Sci* 2007;308(1):231–8.
- [10] Bretherton FP. The motion of long bubbles in tubes. *J Fluid Mech* 1961;10(02):166–88.
- [11] Baroud CN, Tsikata S, Heil M. The propagation of low-viscosity fingers into fluid-filled branching networks. *J Fluid Mech* 2006;546(-1):285–94.
- [12] Weibel ER. *The pathway for oxygen*. Cambridge, MA, USA: Harvard University Press; 1984.
- [13] Stephan K, Pittet P, Renaud L, Kleimann P, Morin P, Ouaini N, et al. Fast prototyping using a dry film photoresist: microfabrication of soft-lithography masters for microfluidic structures. *J Micromech Microeng* 2007;17(10):N69–74.
- [14] Song Y, Manneville P, Baroud CN. Local interactions and the global organization of a two-phase flow in a branching tree. *Phys Rev Lett* 2010;105:134501.